
This is an electronic reprint of the original article.
This reprint may differ from the original in pagination and typographic detail.

Mohammadi, Pezhman; Christopher, Jonkergouw; Beaune, Grégory; Engelhardt, Peter; Kamada, Ayaka; Timonen, Jaakko V.I.; Knowles, Tuomas P.J.; Penttila, Merja; Linder, Markus B.

Controllable coacervation of recombinantly produced spider silk protein using kosmotropic salts

Published in:
Journal of Colloid and Interface Science

DOI:
[10.1016/j.jcis.2019.10.058](https://doi.org/10.1016/j.jcis.2019.10.058)

Published: 15/02/2020

Document Version
Publisher's PDF, also known as Version of record

Published under the following license:
CC BY-NC-ND

Please cite the original version:
Mohammadi, P., Christopher, J., Beaune, G., Engelhardt, P., Kamada, A., Timonen, J. V. I., Knowles, T. P. J., Penttila, M., & Linder, M. B. (2020). Controllable coacervation of recombinantly produced spider silk protein using kosmotropic salts. *Journal of Colloid and Interface Science*, 560, 149-160.
<https://doi.org/10.1016/j.jcis.2019.10.058>

This material is protected by copyright and other intellectual property rights, and duplication or sale of all or part of any of the repository collections is not permitted, except that material may be duplicated by you for your research use or educational purposes in electronic or print form. You must obtain permission for any other use. Electronic or print copies may not be offered, whether for sale or otherwise to anyone who is not an authorised user.



Controllable coacervation of recombinantly produced spider silk protein using kosmotropic salts

Pezhman Mohammadi^{a,*}, Jonkergouw Christopher^b, Grégory Beaune^c, Peter Engelhardt^c, Ayaka Kamada^d, Jaakko V.I. Timonen^c, Tuomas P.J. Knowles^d, Merja Penttilä^a, Markus B. Linder^b

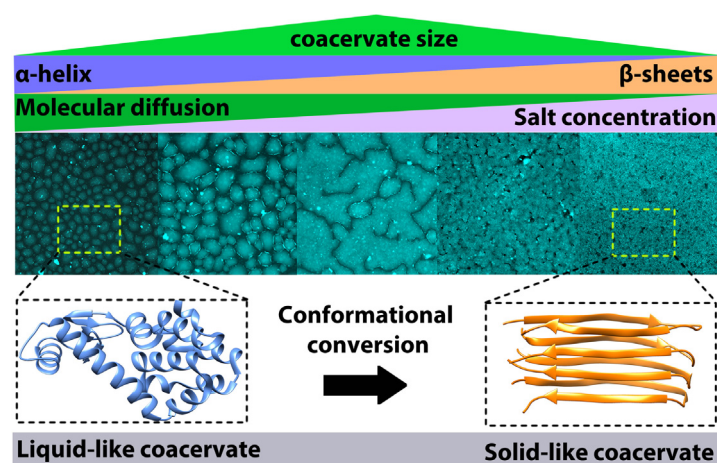
^a VTT Technical Research Centre of Finland Ltd., Espoo FI-02044, Finland

^b Department of Bioproducts and Biosystems, School of Chemical Engineering, Aalto University, P.O. Box 16100, FI-16100 Espoo, Finland

^c Department of Applied Physics, School of Science, Aalto University, FI-02150 Espoo, Finland

^d Department of Chemistry, University of Cambridge, Cambridge CB2 1EW, UK

GRAPHICAL ABSTRACT



ARTICLE INFO

Article history:

Received 31 August 2019

Revised 14 October 2019

Accepted 15 October 2019

Available online 16 October 2019

Keywords:

Liquid-liquid phase transition

Coacervate

Silk-like protein

Genetic engineering

Protein engineering

Salting out

Kosmotropic salt

Classical nucleation theory

ABSTRACT

Recent developments suggest that the phase transition of natural and synthetic biomacromolecules represents an important and ubiquitous mechanism underlying structural assemblies toward the fabrication of high-performance materials. Such a transition results in the formation of condensed liquid droplets, described as condensates or coacervates. Being able to effectively control the assembly of such entities is essential for tuning the quality and their functionality. Here we describe how self-coacervation of genetically engineered spidroin-inspired proteins can be preceded by a wide range of kosmotropic salts. We studied the kinetics and mechanisms of coacervation in different conditions, from direct observation of initial phase separation to the early stage of nucleation/growth and fusion into large fluid assemblies. We found that coacervation induced by kosmotropic salts follows the classical nucleation theory and critically relies on precursor clusters of few weak-interacting protein monomers. Depending on solution conditions and the strength of the supramolecular interaction as a function of time, coacervates with a continuum of physicochemical properties were observed. We observed similar characteristics in other protein-based coacervates, which include having a spherical-ellipsoid shape in solution, an

* Corresponding author.

E-mail address: Pezhman.mohammadi@vtt.fi (P. Mohammadi).

interconnected bicontinuous network, surface adhesion, and wetting properties. Finally, we demonstrated the use of salt-induced self-coacervates of spidroin-inspired protein as a cellulosic binder in dried condition.

© 2019 The Authors. Published by Elsevier Inc. This is an open access article under the CC BY-NC-ND license (<http://creativecommons.org/licenses/by-nc-nd/4.0/>).

1. Introduction

Liquid-liquid phase separation of proteins is important for a wide range of biological functions such as subcellular membrane-less organization, extracellular matrixes, and diseases [1–4]. Phase separation can be explained as a partial dissolution of proteins into dense liquid droplets from a homogeneous solution which is commonly described as condensate or coacervate [5]. There is a growing awareness in many high-performance structural biomaterials that the coacervation of proteins has substantial importance as an intermediate step toward the formation of fibers, adhesives or composites. Sandcastle adhesive [6], tropoelastin [7], squid beak [8], nacre [9], mussel foot adhesive [10], velvet worm adhesive [11], are a prime example of this.

Coacervation of these proteins is a spontaneous assembly process in aqueous solution, either in response to changes in the physico-chemical solution conditions (protein concentration, ionic strength, temperature, and pH), which has been described as one component coacervation, or as the result of neutralization of charged groups by oppositely charged protein species. This is known as complex coacervation. Complex coacervation is either enthalpically or entropically driven assembly, with often a combination of electrostatic, cation- π , and hydrophobic inter-intra interactions driving the phase separation [12,13]. In contrast, one component coacervation is considered an entropically driven phenomenon and it generally depends on hydrophobic interactions [14].

Changes in the ionic conditions have been found to be one of the most influential parameters in the condensation of natural and engineered proteins [7,15–20]. This is because ion specificity and the Hofmeister effect have a substantial influence on the behavior of water molecules (Fig. S1a) [21–23]. Depending on the binding strength of the ionic species, water molecules can be either structured or unstructured in aqueous solution. This can ultimately alter water-water, water-protein, and protein-protein interactions. It is widely recognized that the Kosmotropes exhibit strong bonding interactions with the water molecules, and water can form a strong hydration layer around the ionic species (Fig. S1a) [21–23]. Addition of kosmotropes results in a salting-out effect, by reducing the accessible surface area of the bulk water and making water a poor solvent for the protein. This results in lower protein solubility and higher stability in the aqueous solution by promoting higher inter-intra hydrophobic interactions. This phenomenon has been found to have a substantial importance in the phase separation of biomacromolecules in various biological systems as well as in engineered systems with diverse functionalities [21–23].

One biologically relevant example where kosmotropes play an important role can be seen in the formation of spider silk. Earlier findings suggest the addition of kosmotropes such as phosphate and potassium and a simultaneous reduction of pH and removal of water are the key intermediate steps toward the formation of tough fibers [15,24]. Other works, such as the study of complex coacervation of recombinantly produced mussel adhesive protein in the recent years, have provided great details on how Hofmeister series salt ions can effects the dynamics, structural conformation, interfacial tension and surface adhesion of coacervation [25,26]. Potentially, similar studies could be carried out on different engineered systems to elucidate the effect of Hofmeister series salt.

Particularly, this has immense interest related to the coacervation of other structural proteins such as silk, elastin and resilin [7,27,28].

We previously demonstrated that a recombinantly produced spidroin-inspired 3-block protein architectures called CBM-eADF3-CBM can undergo liquid-liquid phase separation and formation of a one component coacervate [27,29,30]. Design included a mid-block adapted from 12 repeats of load-bearing repetitive residues 325–368 from the sequenced fragment of *Araneus diadematus* major ampulla gland silk fibroin 3, with alternating hydrophobic (poly-A stretches) and hydrophilic (G and Q rich) stretches. This was flanked at the N and C-terminal using an identical protein called cellulose-binding module (CBM). Coacervates formed spontaneously at high protein concentration under low ionic strength [27,29,30]. We also found that the same system can also undergo phase transition and formation of another type of coacervate at high ionic strength. To make a distinction between the two described coacervates, according to differences observed in the physical properties we named them liquid-like coacervate (LLC) and solid-like coacervate (SLC) respectively [27,29,30].

We hypothesize that such distinct differences arise from secondary structure conformation, and by altering the protein concentration versus salts conformation can fine-tune, thus expect the formation of coacervates with the continuum of physico-chemical properties. In this work, we carried out a detailed experimental analysis of the same protein and evaluated how one-component coacervation can be induced with kosmotropic salts. We hypothesize this can be considered as a scalable processing step for pre-molecular self-assembly and structuring of our recombinantly produced protein toward fabrication of protein-based materials with the desired functionality as an adhesive in dried conditions. We demonstrate how kosmotropic salts can be used to accurately control the phase behavior and dynamics of the coacervation assembly with continuum of properties ranging from liquid to solid-like behavior. We gain a detailed understanding of the phase behavior of the recombinantly produced protein and how these differences emerges from secondary structure conformation. We show how accurately dynamics and the structure formation can be controlled at multiple length scales, towards diverse coacervate assemblies with a wide variety of physiochemical properties.

2. Results and discussion

2.1. 3-block silk-like protein undergoes self-coacervation in presence of various kosmotropic salts

In the present work, we systematically exploit the effect of the biologically relevant potassium phosphate salts on the phase-separation of genetically engineered 3-block silk-like protein architecture [27–30]. In addition to that, we tested seven other kosmotropic salts. These were ammonium sulfate, sodium sulfate, ammonium phosphate, sodium phosphate, ammonium acetate, potassium acetate, and sodium acetate. As the first step, we tested sixty-four conditions in which salt versus protein concentration were altered. For the salts, concentrations ranged from 0.05 to 1 M and protein concentrations ranged from 0.058 to 117 μ M. We measured changes in the turbidity of the samples by recording absorbance changes at 600 nm to detect the coacervation, which

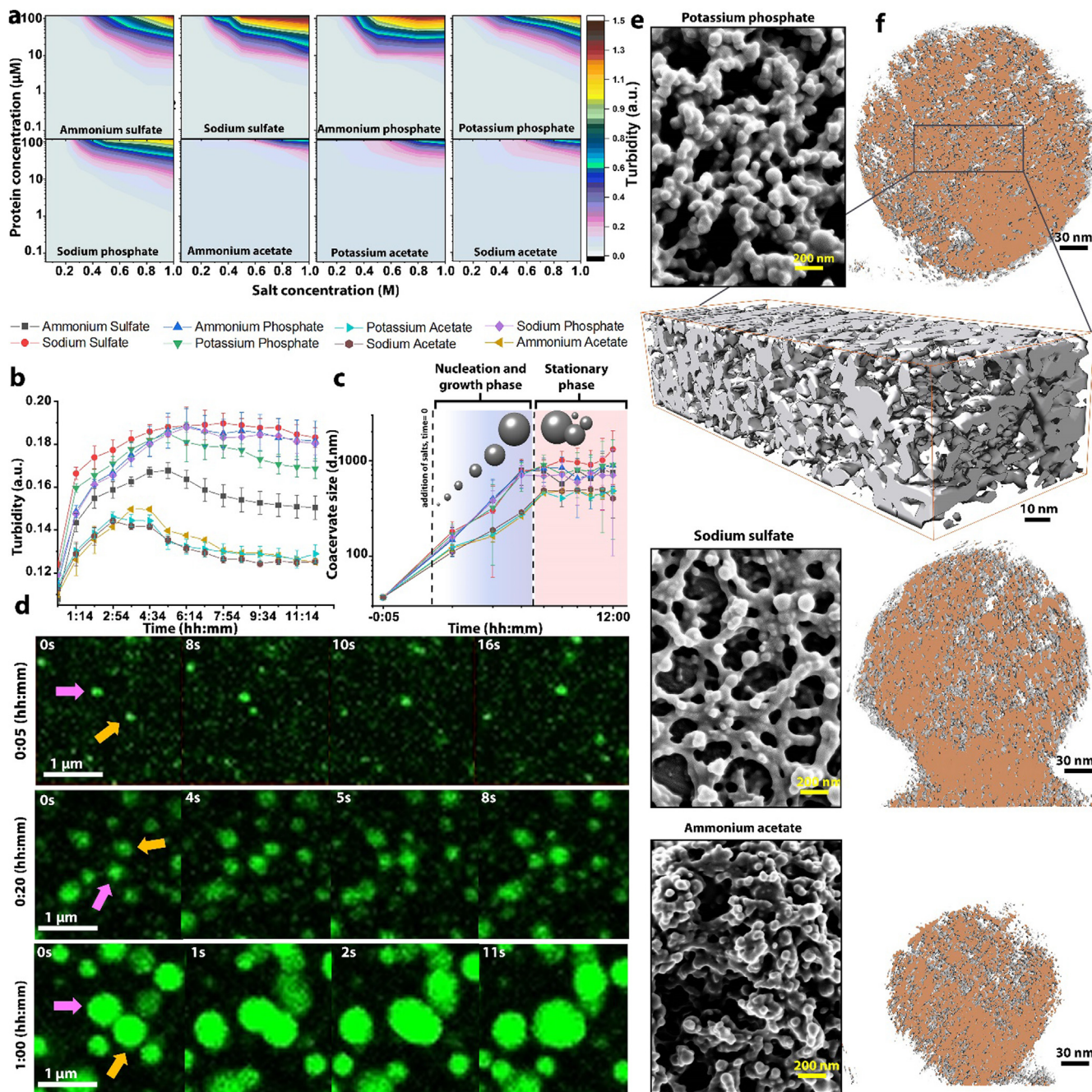


Fig. 1. Self-coacervation of silk-like protein can be initiated by various kosmotropic salts. (a) Coacervation phase diagram of the silk-like protein versus various kosmotropic salts (pH 7), constructed according to the turbidity measurement after twelve-hour incubation. Note that the coacervation process is irreversible at this time point. (b) Changes in the turbidity as the function of time close to the coacervation boundary for all the salt species (protein concentration 5.8 μ M and salts 0.8 M) (N = 3). (c) Mean coacervate diameter measured by DLS for the corresponding samples (N = 30). (d) Confocal scanning microscopy of labeled protein with Oregon Green 488 in a microfluidic device, illustrating the early stage of the growth kinetics and coalescence of the coacervates induced by potassium phosphate as in b and c (Scale bar is 1 μ m). Arrows represent assemblies before the coalescence. (e) Scanning electron micrograph of the early state of coacervation after approximately one-hour into the incubation of protein with potassium, sulfate and ammonium phosphate. It corresponds to the one-hour time point in b and c (Scale bar 200 nm), illustrating clusters of coacervate attached together during the drying process. (f) Five-nanometer slices from the electron tomogram of single coacervates corresponding as in e, illustrating porous interconnected bicontinuous network within for single coacervates (scale bar 30 nm). The rectangular sections illustrate the magnified image of the coacervate made by sodium sulfate (Scale bar 10 nm).

accompanies phase-separation of the silk-like protein in solution, which resulted in the phase-diagram for each salt type at 23 ± 1 °C (Fig. 1a). Intermixing of the highest protein (117 μ M) and salt (1 M) concentrations resulted in an instant turbidity change. In a matter of seconds, this reached a point that one could easily observe the immense transition from transparent to turbid solutions. We noted that not all salts have an equal effect on tur-

bidity. In order, sodium sulfate > ammonium phosphate > sodium phosphate > potassium phosphate > ammonium sulfate > potassium acetate > sodium acetate > ammonium acetate found to have an increasing effect in terms of inducing phase-separation (Fig. S1b). As expected the order of the divalent and monovalent anions follows the classical Hofmeister series, with ammonium sulfate being the only exception. In contrast, monovalent cations

did not follow the Hofmeister series as their counter anion. A simultaneous decrease in the concentration of either protein or salt resulted in less turbid samples. This could reach a point, where no obvious changes could be detected at 600 nm absorbance. In almost all cases, the boundary for the turbidity was found to be at the critical concentration of 1 μM for the protein versus 0.2 M for the salts with a concave up-decreasing coacervation boundary. There was one exception however, 20 μM and 0.3 M was required for all the acetate salts.

2.2. One component self-coacervation of the CBM-eADF3-CBM follows classical nucleation theory

To better understand the start of the assembly and the coacervation kinetics, one concentration combination close to, and one over the phase separation boundary, were selected. This was solely implemented to have not as much rapid increase in the turbidity. This provides slower assembly kinetics for more reliable measurement and better resolution over the longer time period in contrast to higher concentration combinations (Fig. 1b and S2–S9). We selected the protein concentration of 5.8 μM and salt concentration for sulfates and phosphates of 0.8 M (Fig. 1a). However, for the acetates, we needed to select a ten times higher protein concentration (58.8 μM) to be close and over the coacervation boundary. The onset of turbidity was found to be between 0.1 and 0.13 absorbances for all the samples (Fig. 1c). Independent of the salt species, turbidity started to increase gradually over a period of two hours. This continued to increase for all the sulfate and phosphate salts, until the time point of about five hours. After this, a slight decrease in the turbidity was noted, potentially due to partial sedimentation. This was followed by a plateau region and unchanged until the rest of the measurement. Acetate species showed a similar trend, however, with the lowest changes in the turbidity. There is growing evidence that coacervation involves the assembly of proteins into condensed droplets. However, the nature of the assembly mechanism remains unclear with respect to whether it follows the classical nucleation theory, spinodal decomposition or non-classical theory. In our experimental readouts, there is a classical nucleation theory [31–33], in which one can divide the assembly process into two steps of nucleation and growth, followed by a stationary phase (Fig. 1c). Classical nucleation theory is one of the fundamental theoretical model used to describe the kinetics of nucleation with broad applicability in various equilibrium systems [34]. According to this theory, in the early stage of phase separation, our system require (comment: Check that it does not change the meaning of the sentence) to overcome an activation energy barrier and formation of spherical nucleus rich in proteins with the same macroscopic structural features and density [35]. The theory also describes the existence of a sharp interface between the nucleus and the solution, with the protein content increasing rapidly upon the coalescence of neighbouring assemblies (Fig. 1c–f). To our knowledge, this work illustrates the first experimental evidence illustrating protein-based simple coacervation that undertake classical nucleation theory with relevance to the coacervation of other structural proteins such elastin and resilin [27,28].

2.3. Coacervation critically relies on precursor clusters of a few weakly interacting monomers

Following our observation, we performed scattering size distribution analysis on the corresponding samples over the same time period. This enabled us to get a direct readout of the nucleation step and determine roughly hydrodynamic diameters of the coacervates and correlated that to the changes in the turbidity of the samples. Surprisingly, we found that even in non-coacervated con-

ditions, CBM-eADF3-CBM solutions have precursor clusters with an average size of about 35 nm (Fig. 1c). We found this value to be higher than what would be predicted for monomers (~10 nm), and suggest that these are the clusters of 3 to 4 weakly interacting monomers. Such cluster size distributions can be expected for a so-called super-saturated system in the first order phase transition described in the classical nucleation theory [33,36]. In such a system, there exists a nucleation barrier and a critical size above which precursor clusters grow and mature as a function of time in response to changes in the solution condition. If the system does not pass the nucleation barrier and the critical cluster size distribution, condensation will not occur.

To test that this phenomenon also applies in our system, we looked at a concentration above and below the phase separation boundary. We tested this by keeping the protein concentration the same (5.8 μM in case of sulfates and phosphates and 58.8 μM in case of acetates) while altering the salt concentration to cross the phase separation boundary. We selected 0.2 M as the salt concentration in which no phase separation was observed and 0.8 M as the salt concentration in which we noted phase separation occurs in the given protein concentrations for all the salt species. After addition of 0.2 M salt, we observed the formation of assemblies with the average sizes ranging between 50 and 65 nm (Fig. S10). This remained unchanged and below 100 nm during the rest of the measurement for all the salt species. Addition of 0.8 M salt, on the other hand instantly initiated the formation of much large protein assemblies. Already after a few minutes into the equilibration, assemblies with the sizes of about 100–150 nm were observed. Over the next two hours, we noted that these assemblies gradually grew up to around 300–700 nm through the recruitment of other dispersed weakly interacting protein clusters from the solution and coalescence of the smaller coacervates (Fig. 1d and S11), after which the system reaches an equilibrium state. With this, we defined the approximate nucleation barrier and critical cluster size distribution over which condensation will occur in our system to be 100–150 nm. With this, we provided the first experimental evidence of the critical cluster size distribution and nucleation barrier of a protein-based simple coacervated system in a super-saturated system in the first order phase transition described in the classical nucleation theory [33,36]. Furthermore, a constant increase of the droplet size implies no redissolution of the proteins in the droplet with the surrounding solution and formation of structurally stable assembly in the solution. High-resolution electron microscopy and 3D reconstruction of individual coacervates assemblies revealed the formation of the heterogeneous interconnected bicontinuous network (Fig. 1e, 1f and video 1), which has been found to be one of the main characteristics of coacervated protein in a natural or engineered system [27,28,37–39]. Looking at the data points during the stationary phase, we noted an increasing standard deviation leading to the point that measurements could not be performed. As the coalescence becomes a diffusion-limited process, which results in the formation of non-uniformly sized droplets, the DLS typically has low-resolution for samples with a large polydispersity index (Fig. S12).

2.4. Coacervation involves a time-dependent conformational conversion

To monitor possible conformational transitions of a coacervate during nucleation-growth in the stationary phase, we used Thioflavin T (ThT) dye. ThT has a specific binding affinity for the β -sheet structures of proteins and can be used as a detection marker [40,41]. Upon binding, ThT exhibits enhanced fluorescence intensity at 492 nm, characteristic for the formation of β -sheet structures after addition of the salts (Fig. 2a). Independent of the salt type we

maturity and kinetic arrest for the coacervates over time. Furthermore, looking at the effect of each salt species, not all have the same effect on the conformational transition. Sodium sulfate and ammonium acetate were found to be the most and least influential salts respectively, where every other salt fell in between these two (Fig. 2a and S14).

From the turbidity measurement, we anticipated a range of conformational conversions in response to the changes in solution conditions. Fig. 2b and S15–21 illustrates fluorescence microscopy images, corresponding to the concentration combination used in turbidity measurement. We found considerable differences in the fluorescence intensity signal. Increasing concentration of salt resulted in a greater degree of structural changes and the formation of coacervates with high β -sheet content. Moreover, the highest salt concentration led to a faster transition rate and resulted in higher β -sheet signals independent of protein concentration (Fig. S22). In contrast, we noted a dramatic decrease in the rate and dynamics of the transition and overall β -sheet content if the salt concentration was lowered. For the lowest content of salt,

we found this structural conversion become minimal and the proteins mostly retained their α -helical conformation with a relatively small amount of β -sheet (Fig. 2b).

To identify the initial conformation of the protein and re-evaluate the observations made by ThT assay, we performed circular dichroism (CD) (Fig. 2c). We found that the initial solution conformation to be predominantly α -helical. This can be identified from the negative signatures bands at ~ 210 and ~ 223 nm. Addition of salt resulted in a shift toward a single negative band. One hour into the incubation, this band shows around 230 nm. However, we noted a gradual shift towards ~ 225 nm after five hours, which remained unchanged throughout the rest of the experiment. This can be interpreted as β -sheet conformation, with the difference that the band for a typical protein having a β -sheet conformation falls between 210 and 223 nm. Such lower spectra have been observed for partially soluble assemblies with intrinsic long-range β -sheet conformation, as in amyloid- β fibrils [42]. These observations were in agreement with the ATR-FTIR measurement of the dried protein samples, with a clear shift for the

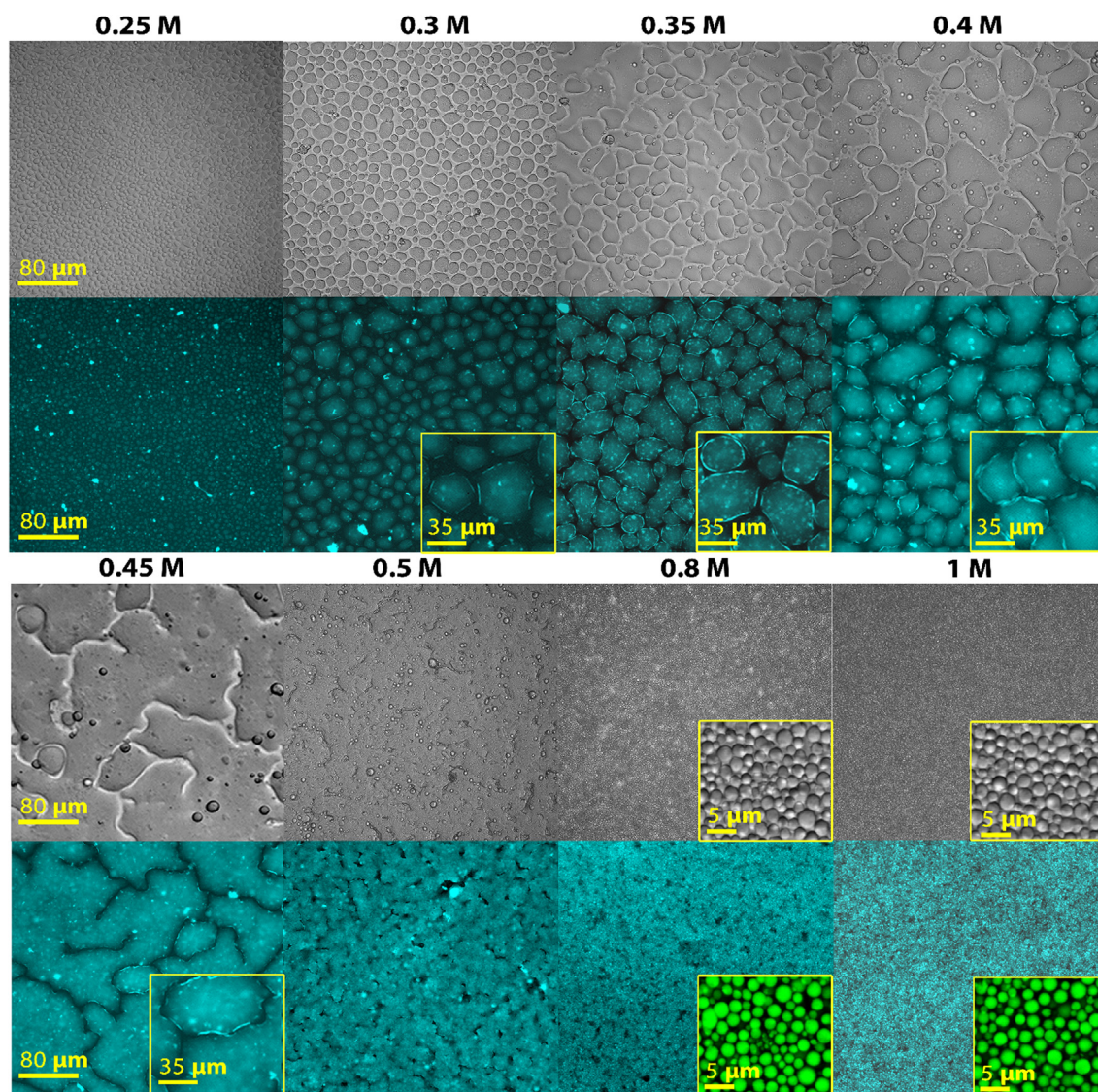


Fig. 3. Morphologically diverse coacervate assemblies in response to changes in the salt concentration. Bright field and fluorescence microscopy (ThT stained) images, illustrating the effect of potassium phosphate concentration on the morphology of the coacervate after twelve hours incubation (protein 117 μ M, salt concentration 0.25–1 and the scale bar for all the images 80 μ m) on the surface of glass. For the 0.8 and 1 M salt combinations, higher magnification bright field and fluorescence microscopy (labeled with Oregon Green 488) images are shown, illustrating the close-packed array of ~ 2 –3 μ m coacervates. Yellow boxes illustrate areas with higher magnification. Note, bright field images do not correspond to exactly same area/sample as the fluorescence images.

amide I band from 1635 (dominantly α -helical) to 1622 (β -sheet) (Fig. 2d).

Using multiple prediction programs (Fig. 2e), we then searched for the structured region in the primary sequence of the spider silk originated repetitive block. This was carried out by computing the average flexibility, buried residues, as well as coil and alpha-helix scale profiles in the form of 2D plots for residues 325–368 of *Ara-nes diadematus* spidroin 3 [43–45] and by assigning numerical values to each amino acid. The results suggested that domains containing poly-alanine stretches, display a propensity for α -helical conformation. Previously, NMR in pure solution has been used to identify molecular interactions among macromolecular components, as well as to determine the structure of subunits that undergo liquid-liquid phase separation [46,47]. However, the structural organization of coacervate droplets using solution-state NMR was challenging to identify due to the reduced diffusion of molecules, the high viscosity of the solution and the gradual sed-

imentation of coacervate droplets due to the long measurement time [48]. Instead, solid-state NMR has previously been employed to study the structural organization of protein-based hydrogel and fibrillar assemblies in hydrated state that are very similar to the coacervated system [49–52]. Here, we combined solution and solid-state NMR spectroscopy to obtain an atomic-level insight into the poly-alanine conformation before and after coacervation by discriminating between the peaks corresponding to alanine C α and C β . The chemical shift for ^{13}C was found to be sensitive to slight differences in the structural conformation. Fig. 2f illustrates the comparison of ^{13}C NMR spectra (aliphatic part) of the silk-inspired protein before and after coacervation, demonstrating the chemical shift for the Alanine C β and C α . The alanine shows strong peaks at 52.98 and 16.28 ppm. These correspond respectively to C α and C β of Ala residues in the α -helical conformation [53–55]. In contrast, after coacervation, we noted a clear shift (C α = 49.98 ppm and C β = 21.26 ppm) for both carbons, which

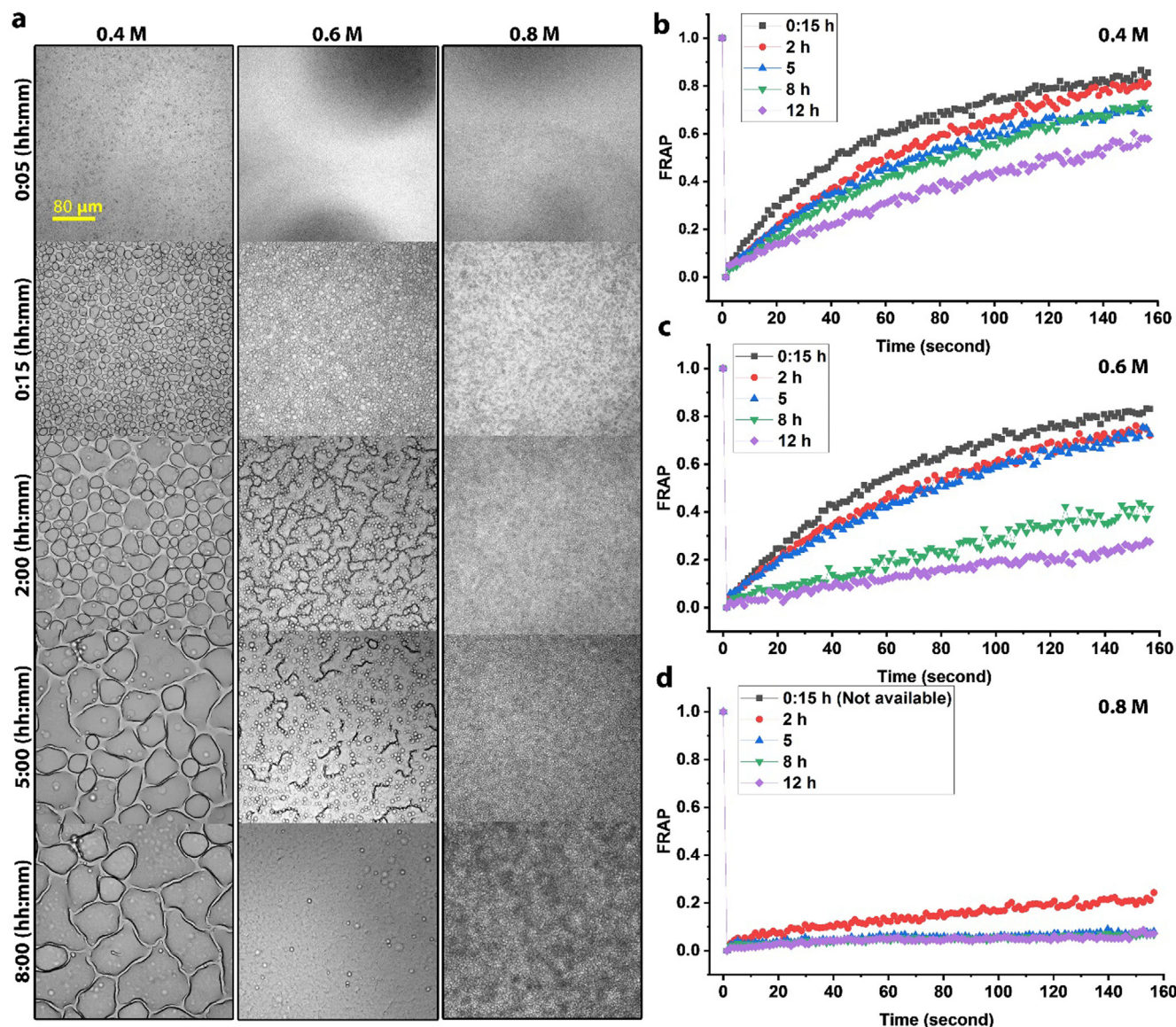


Fig. 4. Physical characteristics of the coacervates strongly depend on the concentration of salt and their maturity time. (a) Bright field microscopy images of the coacervation over eight hour time period, illustrating maturation of the fixed protein concentration (117 μM) into various coacervate assemblies in low, medium and high potassium phosphate concentrations. (b–d) Fluorescence recovery after photobleaching (FRAP) curves for the corresponding condensates (labeled protein with Oregon Green 488) as in a. ROI = 2 μm circular area; FRAP recovery was normalized to one in all cases.

was previously associated with conformational conversion of Ala residues to β -sheet [53–55].

To summarize, we tested the molecular structuring of coacervates in solution, semi-hydrated and dried state using four different techniques. Combining all the results, we find very clear evidence for conformational conversion as a progressive event taking place throughout the nucleation, growth and maturity steps of the coacervate in this study.

2.5. Diverse coacervate assemblies with different physical properties

At high protein concentrations ($\sim 117 \mu\text{M}$), we noted the formation of various coacervate assemblies with diverse morphological characteristics in response to changes in the salt concentration (Fig. 3). For potassium phosphate, three very distinct assemblies could be observed unlike other salt species. Independent of surface chemistry, the same phenomena could be observed on both hydrophilic (glass) and hydrophobic (polystyrene) surfaces (Fig. S24). From 0.25 to 0.45 M, coacervates with ellipsoid shapes were formed while maintaining their individual integrity. We noted that the shape of the coacervates became more irregular and spread after an increase in protein concentration. Depending on the concentration of the potassium phosphate, the sizes of these assemblies ranged from ~ 20 to $300 \mu\text{m}$. Between 0.5 and 0.6 M, we noted the protein can fully phase separate into a single continuous phase after wetting and spreading on the substrate. Above 0.6 M, we only observed the formation of coacervates with sizes about $2\text{--}3 \mu\text{m}$ clustered to form a multilayer film. One interesting observation for coacervates induced using lower salt concentrations was that the ThT fluorescence signal was distinctly stronger at the circumference while having lower intensity in the core of the condensates (Fig. 3). This was distinctly different from higher salt concentrations, in which the ThT signal observed uniformly throughout the assemblies. We found such a feature to be more evident at 0.35 and 0.45 M. A likely explanation is global reduction of the conformational entropy while increasing the structure formation mainly at the interface of the assemblies that are more exposed to the potassium phosphate in the solution. Upon an increase in the salt concentration this feature propagates through the entire protein network to form a uniform β -sheet rich structural conformation.

To investigate what the key intermediates steps are toward the formation of such unique structures, we selected three salt combinations (0.4, 0.6 and 0.8 M) as in Fig. 4a and video 2 and followed their assembled steps over an eight hour time period. In all cases, we found that the assembly initiates through the formation of spherical/ellipsoid-shaped coacervate droplets while being suspended in the solution. Coacervates started to form instantly while being suspended in solution. This was independent of the salt concentration. As the coacervates grew large ($1\text{--}2 \mu\text{m}$), we noted they respond to gravitational forces and began to sediment from the bulk suspension on a timescale of minutes. We noted coacervates are subjected to both Brownian motion, as well as a constant gravitational pull. This results in coalescence (Fig. 4b and video 2) of the coacervates as they collide and wet the surface simultaneously. Even though the start of the assembly remained the same in all cases, we noted that the intermediate kinetic steps for low, medium and high salt concentrations are considerably different. For 0.4 M salt, the size of the assemblies increased constantly over an eight hours time period (video 2). In the case of 0.6 M salt, after only two hours of incubation, coacervates were assembled into a continuous phase. In the next six hours, we found that almost all the coacervate droplets suspended in the solution were recruited into the continuous phase on the substrate (video 2). In contrast to low and medium salt concentrations, coacervates triggered by high salt remained morphologically unchanged after fifteen min-

utes, which over time formed a thick clustered layer on the surface by a close-packed array of $\sim 2\text{--}3 \mu\text{m}$ spherical coacervates (video 2).

Since condensation of the protein was found to be time-dependent in regards to conformational conversion, we anticipated depletion in the fluidity of the coacervate with the increase in the net inter-molecular attractive forces mediated by the addition of kosmotropic salts. For that, we followed the evolution of the inter-molecular network and alteration in the mesoscale diffusion dynamics within the coacervates over the same time period as in Fig. 4b, using fluorescence recovery after photobleaching (FRAP). Data obtained from the FRAP measurement showed two very separated trends. First, with the increase in salt concentration, we found a substantial decrease in diffusion dynamics in a very early stage of condensation (Fig. 4c). From 0.4 to 0.8 M, the diffusion rate decreased approximately three fold. Second, diffusion decreased as the coacervates were incubated for a longer time period. We found that the coacervates move from liquid-like to more solid-like characteristics. This was independent of salt concentration, with the difference that assemblies with 0.8 M salt reached to a kinetically arrested state faster. They also display more prominent characteristics as seen in a hard gel due to physical crosslinking from β -sheet and formation of the bicontinuous network. A similar trend has been associated with membraneless organelles and their development toward diseases [56,57]. It has been illustrated that if the strength of the inter-molecular interactions within the protein-rich condensate increases, this can cause the fluid assembled to gradually transform into a hard protein gel, aggregates, and even crystals.

2.6. Using the coacervate as a cellulose binder

Earlier we demonstrated that coacervates of CBM-eADF3-CBM induced by changes in the protein concentration show properties that are suitable for binding different cellulosic substrates in the dried state [27,29,30]. Based on FRAP measurement we found that coacervates induced by 0.4 M potassium phosphate display very similar physiochemical characteristics. Therefore, we explored similar possibilities in this study. To test adhesive characteristics of coacervates we induced bulk phase separation. Phase separation instantly started and the dense phase of the solution containing the coacervates was settled at the bottom of the tube by applying centrifugal forces, while the dilute supernatant phase of the protein solution remained at the top (Fig. 5a). After this, $30 \mu\text{l}$ of the dense phase was applied on a 1 cm^2 joint, allowed to solidify and cure at ambient conditions after water evaporation to form the joint. We used bacterial cellulose (BC) as the primary substrate. BC was selected for two main reasons. Firstly, it is entirely made from cellulose and we anticipated stronger affinity of the CBM-eADF3-CBM to a purely base cellulosic substrate. Secondly, BC has remarkable stiffness and strength, enabling greater mechanical load on the adhesive matrix before catastrophic failure. Bond strength varied between 2 and 24 N/cm^2 depending on the dry mass content of the adhesive (Fig. 5b). Of all samples, 1 mM showed the highest bond strength of $24 \text{ N/cm}^2 \pm 5$, while decreasing the mass of adhesives resulted in a substantial decrease in the bond strength. This reached to the point that we were not able to record any forces for the lowest concentration (0.1 mM) as the dense phase formed a very weak joint. Comparing to the earlier effort, in which LLC were used for binding the same substrate, we noted salt induced coacervate exhibit lower strength and but also lower work of fracture, corresponding to the area under the fracture curve. [27,29,30] Such changes could be explained due to conformational differences between the two coacervate types. In which LLC exhibit amorphous nature with low or close to none β -sheet content [27,29,30]. This enables the adhesive matrix to dissipate greater energy before catastrophic failure. Whereas salt

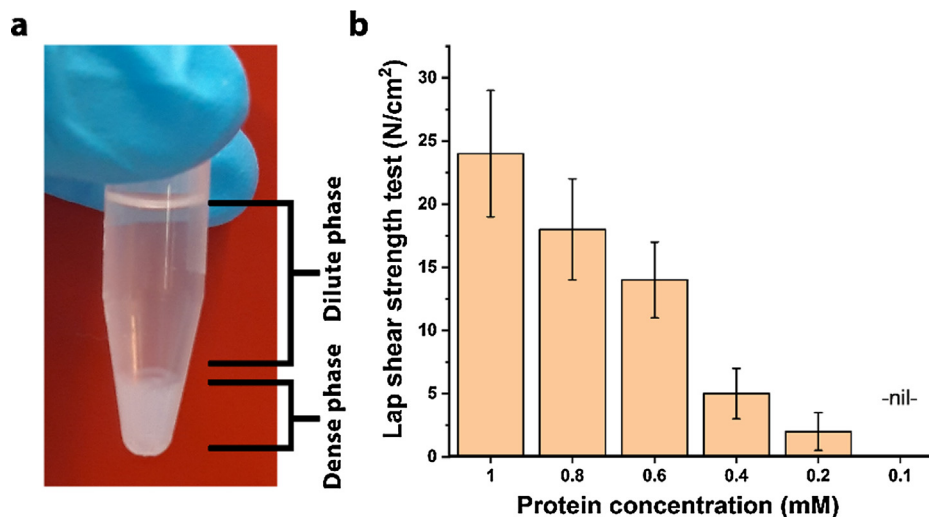


Fig. 5. Adhesive characteristics of the salt-induced coacervates. (a) Bulk phase separation of CBM-eADF3-CBM (1 mM) induced by potassium phosphate (0.5 M) after centrifugal force separating the solution into the dense and dilute phase. (b) The calculated mean and standard deviation of the lap-shear strength test of bacterial cellulose that was glued by the dense phase containing coacervate of CBM-eADF3-CBM with at various concentrations (N = 5). (c) The calculated mean and standard deviation of the lap-shear strength test of the 1 mM protein concentration at different pH for the corresponding dense phase as in a (N = 5).

induce coacervate show some degree of conformational conversion from amorphous to semi-crystalline, thus stiffer adhesive matrix.

3. Conclusions

In the present work, we analyzed the coacervation of recombinantly produced spidroin, inspired by a 3-block architecture, in a wide range of kosmotropic salts in vitro. Conditions were carefully controlled, which allowed us to systematically characterize the dynamics of the start, intermediate and later stages of assembly through a combination of different microscopy techniques and spectroscopy measurements. This led us to structurally and functionally different coacervate assemblies at various concentrations of protein versus salt. Independent of the salt species, we found that the self-assembly of the coacervates accompanies classical nucleation theory and critically relies on precursor clusters of a few weak-interacting monomers. We followed early stages of nucleation close to the coacervation boundary (low protein concentration) and noted assembly initiates at nanometer length scales through recruitment of precursor clusters from the surrounding solution. Once the condensates reach a critical size, we observed they undergo uncontrollable growth, by coalescing with the other condensates to form larger coacervates. We found that coacervation kinetics involves a time-dependent conformational conversion of the protein from α -helical/random-coils to more β -sheets. We showed that poly-alanine stretches in the load bearing repetitive region are the primary sequences undergoing this transition. Over the coacervation boundary, at much higher protein concentrations, coacervates with diverse behavior were observed. These ranged from the rapid restriction of droplet growth, extensive clustering and maintaining individual droplet integrity, gravitational sedimentation and surface wetting and spreading upon contacting to both hydrophobic and hydrophilic substrates. Many of the observations we report here could be a generic property for many other existing molecularly engineered structural proteins. Future development could focus on altering amino acid sequences and block architecture for more robust assemblies and functionalities. This could also likely bring new understanding to the overall question of functional assembly in protein-based biomaterials. We think the results presented here in this work could have a substantial relevance in the diverse area of soft matter

research [58], with implications in practical applications such as coatings, adhesives and composites.

4. Materials and methods

4.1. Cloning, protein production, and purification

Cloning, protein expression, and protein purification carried out as described previously [27,29,30]. Shortly, genes encoding twelve time repeats of residues 325–368 of *Aaraneus diadematus* spidroin 3,[43–45] gene sequence encoding cellulose binding module from *Ruminiclostridium thermocellum*,[59] and gene sequences encoding the C-terminal and N-terminal linkers of spidroin 1 from *Euprosphenops australis* [60], were codon optimized and synthesized by GeneArt gene synthesis for expression in *E. coli*. Fusion constructs assembled using seamless golden gate cloning [61–63], in a conventional pE-28a (+) (kanamycin resistance) expression vector six histidine purification tag at the C-terminal. MagicMedia™ was used as the expression media. For purification, either HisTrap columns were used or for larger scale purification cell lyse were heated for 30 min at 70 °C to precipitate other proteins except for the silk-like fusion constructs. Proteins were then desalted using Econo-Pac gravity flow column using Milli-Q water. This was followed by an additional wash (3 times) using 50,000 molecular weight cut-off vivospin centrifugal concentrators to remove the lower molecular weight of truncated silk-like fusion protein that was co-purified alongside of the intact silk-like fusion constructs during the purification step. Samples were then stored in –80 °C until use.

4.2. Hofmeister ions

In the present work, the coacervation of a protein inspired by spider silk was studied with the common series of Hofmeister salt ions. All salts, including K_2HPO_4 , Na_2HPO_4 , $(NH_4)_2 PO_4$, Na_2HSO_4 , $(NH_4)_2SO_4$, KCH_3CO_2 , $NaCH_3CO_2$ and $NH_4CH_3CO_2$, were purchased from Sigma-Aldrich with the purities grade ranging from 98% to 99.5% unless otherwise stated in the text. All the salt solutions with the desired concentrations were prepared in a 10 mM Tris-HCL buffer (pH 7.4). All the salt solutions were prepared fresh before

each measurement. Note: Tris-HCL buffer alone did not trigger coacervation of the protein.

4.3. Turbidity measurement

Coacervation detected by measuring changes in the turbidity of the samples at 600 nm (OD_{600}). This was carried out using Synergy™ H1 multi-mode microplate reader. The coacervate amount in a sample approximated to be proportional to its OD_{600} . Samples were prepared directly into 96-well plates, by mixing one to one ratio of protein to salt in the desired final concentrations with the final volume of 200 μ l. The temperature was kept close to the room temperature (23 ± 1 °C). Before every readout, samples were shaken for 2 s. As the blank, the same volume of Milli-Q water was used. Backgrounds were subtracted from the measurement readouts.

4.4. Dynamic light scattering (DLS)

DLS carried out using a temperature controlled (23 ± 1 °C) Malvern Zetasizer Nano-ZS90 equipped with a He-Ne laser (633 nm) at 90° backscattering angle. For each sample, 30 measurements carried out and the result illustrated as mean with standard deviation.

4.5. Thioflavin T (ThT) assay

ThT (Sigma) was dissolved in Milli-Q water and centrifuged at $16,000 \times g$ for 20 min and then filtered through a 0.2 μ m syringe filter to make 1 mM stock solution. For the measurement of ThT fluorescence was diluted with water and added to the protein solutions in working concentration of 0.05 mM in the absence of salt. Protein and ThT solutions were equilibrated at 23 ± 1 °C for 15 min before adding appropriate salt concentrations to the protein-ThT solutions. Fluorescence measurements carried out using Synergy™ H1 multi-mode microplate reader through the bottom of the 96 well plates with the excitation 450 nm and emission of 492 nm at room temperature (23 ± 1 °C). As the control, same volume and concentration of ThT were made in combination with protein and absence of salt, in the salt solutions in the absence of protein and in Milli-Q water. Backgrounds were subtracted from the measurement readouts.

4.6. Attenuated total reflectance Fourier transform infrared spectroscopy (ATR-FTIR)

ATR-FTIR carried out using a Unicam Mattson 3000 FTIR spectrometer equipped with PIKE Technologies GladiATR with diamond crystal plate. Before the measurement, non-coacervated and all the salt-induced coacervated samples were dried for a minimum of 12 h. This was done to minimize the noise from water molecules. All the samples were then scanned for 120 in absorbance mode within the range of $400\text{--}4000$ cm^{-1} , with a resolution of 2 cm^{-1} .

4.7. Optical and fluorescence microscopy

Multiple platforms were used to visualize the coacervates.

(1) Axio Observer inverted microscope (Zeiss,) equipped with a motorized stage and AxioCam MRm camera (Zeiss), a $\times 100$ /numerical aperture was used for fluorescence imaging of the coacervates. (2) Nikon Eclipse Ti equipped with Andor Zyla sCMOS camera and $\times 40$ objective for bright field imaging of the coacervates. (3) Leica TCS SP5 confocal microscope equipped with $\times 100/1.2$ water objective was used for studding the nucleation and growth of the coacervates. Images were taken either in fluorescence, phase con-

trast or bright field mode. Images were further processed with ImageJ [64].

4.8. Circular dichroism (CD)

CD spectra were collected on a temperature controlled Chirascan™ CD (23 ± 1 °C), using a QS quartz cuvette with 1 mm path length. Data acquisition was performed in the wavelength range 190–260 nm and 1 nm bandwidth, with 1 nm steps and averaging time of 0.5 s. We repeated eight-time every measurement, which was then averaged and smoothed.

4.9. Fluorescence recovery after photobleaching (FRAP)

Lysine amino acids of the terminal CBM labeled using Oregon Green 488 (carboxylic acid, succinimidyl ester, 6-isomer), according to instructions provided by the distributor (Thermo Fisher). FRAP experiment carried out by using Leica TCS SP5 confocal microscope with FRAP booster (Leica DM5000) and a DD488/561 dichroid beam splitter at 63x/1.2 water objective. Samples were bleach using a laser at 488 nm. Intensity traces were collected using Leica AF Lite -TCS MP5, after passing the emission through 88/561 dichroid and detected by a photomultiplier. Intensities were corrected for photobleaching and normalized with pre-bleaching.

4.10. Scanning electron microscopy (SEM)

Scanning electron microscopy (SEM) performed with a Zeiss FE-SEM field emission microscope with variable pressure, operating at 1–1.5 kV. Otherwise states, all the samples were sputtered and coated with a thin platinum layer prior to imaging. For further analysis and image processing software package ImageJ [64] and ImageJ Fiji (versions 1.47d) [65] was used.

4.11. Scanning transmission electron microscopy (STEM)

Scanning transmission electron microscopy carried out using JEM-2800 Transmission Electron Microscope operated at 200 kV in a bright/dark field mode. Sample preparation was carried out by using 200 mesh carbon (CFT200-Cu) or Quantifoil 3.5/1 holey carbon copper grids with 3.5 μ m holes which were cleaned using a Gatan Solarus 9500 plasma cleaner.

4.12. Microfluidics fabrication

The microfluidic device was fabricated through standard UV-lithography technique. Briefly, a 50 μ m thick negative photoresist (SU-8 3050, MicroChem) was spin-coated on a silicon wafer. After that, a photo mask was placed onto the wafer and exposed to UV light in order to promote the polymerization of the photoresist. The master was developed using propylene glycol methyl ether acetate (PGMEA, Sigma-Aldrich) to remove the excess of photoresist.

4.13. Bioinformatics analysis

The structural predictions on the amino acid sequence carried out using ProtScale [66]. This was carried out by computing average flexibility, buried residues, coil and alpha-helix scale profile in form of 2D plots for residues 325–368 of *Aaraneus diadematus* spidroin 3 [43–45] by assigning numerical values to each amino acid.

4.14. Scanning transmission electron (STEM) tomography

Samples were vitrified by plunging 5 μl of the suspension into a mixture of propane and ethane (-180°C). Samples were then handled under liquid nitrogen and transferred into a FreeZone 4.5 Liter Cascade Benchtop Freeze Dry Systems equipped with collector cooling chamber at -105°C .

STEM tomographic tilt series were acquired using analytical STEM JEOL JEM-2800 microscope. Samples were tilted between $\pm 72^\circ$ angles with 8° increment steps. IMOD was used for cross correlation alignment. Maximum entropy method (MEM) reconstruction scheme, with custom made program on Mac with regularization parameter value of $\lambda = 1.0\text{e}-3$. Chimera software package was used for visualization.

4.15. Bacterial cellulose preparation

Bacterial cellulose produced using *Acetobacter xylinum* grown in Schramm and Hestrin (HS) medium as described previously. The synthesized cellulose washed by addition of 200 mM NaOH solution for 48 h. Samples were then washed several time with MQ water until turned white. The bacterial cellulose was then stored in water at $+4^\circ\text{C}$ until they dried under ambient conditions.

4.16. Nuclear magnetic resonance (NMR) spectroscopy

Alanine C α and C β chemical shifts were assigned according to HSQC ^{13}C - ^1H correlation NMR spectra for non-coacervate samples and HETCOR ^1H - ^{13}C correlation NMR spectra for the coacervated samples. HSQC spectrum was recorded with a Bruker AVANCE III 500 NMR spectrometer with magnetic flux density of 11.7 T, equipped with a 5 mm BBFO probehead with inverse geometry. The sample was dissolved in 1:1 $\text{D}_2\text{O}:\text{H}_2\text{O}$, with a concentration of 20 mg/ml. A region selective sensitivity enhanced pulse program that utilizes adiabatic pulses on carbon channel was used in acquisition (shsqcetgpsisp2.2). Recorded spectral width for proton was 13 ppm, with midpoint of the spectrum at 4.7 ppm. The excitation range for carbon was 70 ppm, centered at 45 ppm. The average value for one-bond J-coupling between protons and carbons was set as 145 Hz. Four scans were recorded for each 512 increments in the indirectly detected dimension, delay between successive scans was 1.5 s, and acquisition time was 200 ms. Apodization with Gaussian window functions was used for both dimensions. The ^{13}C spectrum was recorded with a pulse program utilizing an additional adiabatic flip-back pulse in order to remove the need for long relaxation delays (Bruker pulse program 'UDEFT'). Spectral width was 220 ppm, acquisition time 360 ms, and 4096 scans with a 1.5 s repetition delay were recorded. The solid-state spectra recorded at a MAS frequency of 12.5 kHz. A linear ramp from 49.0 to 61.2 kHz radio-frequency (RF) field amplitude on ^1H and 65.8 kHz amplitude on ^{13}C was used for CP, 0.5 ms. Spinal 64 decoupling was applied during acquisition with a ^1H RF field amplitude of 83.3 kHz and a pulse length of 5.8 μs . The acquisition time was 10 ms. The recycle delay was 2.5 s. All data was processed using Bruker BioSpin's TopSpin 3.6 software

4.17. Lap shear adhesive test

Lap-shear adhesive strength test carried out by inducing bulk phase separation using potassium phosphate (0.4 M) at various pH ranging from 5.5 to 8.5. In order to minimize the effect of crystallization of the potassium phosphate on the adhesive strength of the BC joint, supernatant was removed (Fig. 5a) and the dense phase was washed with MQ water. About 30 μl of dense phase spread over the area of 1 cm^2 and allowed to dry at ambient conditions for minimum of 24 h under 1 kg weight. Before adhesion

test, all the specimens were equilibrated in a humidity controlled chamber at 50% RH and room temperature overnight otherwise as stated in the text. Lap-shear strength test performed using a 5kN tensile module (Kammrath & Weiss GmbH, Germany) using a 100 N load cell with the elongational speed of 2 $\mu\text{m}/\text{second}$.

Author contributions

The manuscript was written through the contributions of all authors. All authors have approved the final version of the manuscript.

Acknowledgement

This work is supported by Academy of Finland through its Centres of Excellence Programme (2014–2019) and Jenny and Antti Wihuri Foundation (Centre for Young Synbio Scientists).

Appendix A. Supplementary material

Supplementary data to this article can be found online at <https://doi.org/10.1016/j.jcis.2019.10.058>.

References

- [1] M.-T. Wei, S. Elbaum-Garfinkle, A.S. Holehouse, C.C.-H. Chen, M. Feric, C.B. Arnold, R.D. Priestley, R.V. Pappu, C.P. Brangwynne, Phase behaviour of disordered proteins underlying low density and high permeability of liquid organelles, *Nat. Chem.* 9 (2017) 1118.
- [2] M.-T.S. Wei, C.P. Brangwynne, Sequence determination of liquid-liquid phase-separated assemblies of engineered disordered proteins in living cells, *Biophys. J.* 116 (2019) 454a.
- [3] C.P. Brangwynne, P. Tompa, R.V. Pappu, Polymer physics of intracellular phase transitions, *Nat. Phys.* 11 (2015) 899–904, <https://doi.org/10.1038/nphys3532>.
- [4] S. Alberti, A. Gladfelter, T. Mittag, Considerations and challenges in studying liquid-liquid phase separation and biomolecular condensates, *Cell* 176 (2019) 419–434.
- [5] A.A. Hyman, C.A. Weber, F. Jülicher, Liquid-liquid phase separation in biology, *Annu. Rev. Cell Dev. Biol.* 30 (2014) 39–58, <https://doi.org/10.1146/annurev-cellbio-100913-013325>.
- [6] R.J. Stewart, C.S. Wang, I.T. Song, J.P. Jones, The role of coacervation and phase transitions in the sandcastle worm adhesive system, *Adv. Colloid Interface Sci.* 239 (2017) 88–96.
- [7] G.C. Yeo, F.W. Keeley, A.S. Weiss, Coacervation of tropoelastin, *Adv. Colloid Interface Sci.* 167 (2011) 94–103, <https://doi.org/10.1016/j.jcis.2010.10.003>.
- [8] Y. Tan, S. Hoon, P.A. Guerette, W. Wei, A. Ghadban, C. Hao, A. Miserez, J.H. Waite, Infiltration of chitin by protein coacervates defines the squid beak mechanical gradient, *Nat. Chem. Biol.* 11 (2015) 488–495.
- [9] S.Y. Bahn, B.H. Jo, Y.S. Choi, H.J. Cha, Control of nacre biomineralization by Pif80 in pearl oyster, *Sci. Adv.* 3 (2017) e1700765.
- [10] J.H. Waite, Mussel adhesion – essential footwork, *J. Exp. Biol.* 220 (2017) 517–530, <https://doi.org/10.1242/jeb.134056>.
- [11] A. Baer, S. Schmidt, S. Haensch, M. Eder, G. Mayer, M.J. Harrington, Mechanoresponsive lipid-protein nanoglobules facilitate reversible fibre formation in velvet worm slime, *Nat. Commun.* 8 (2017) 974.
- [12] L.-W. Chang, T.K. Lytle, M. Radhakrishna, J.J. Madinya, J. Vélez, C.E. Sing, S.L. Perry, Sequence and entropy-based control of complex coacervates, *Nat. Commun.* 8 (2017) 1273.
- [13] D. Priftis, N. Laugel, M. Tirrell, Thermodynamic characterization of polypeptide complex coacervation, *Langmuir* 28 (2012) 15947–15957.
- [14] S.E. Reichheld, L.D. Muiznieks, F.W. Keeley, S. Sharpe, Direct observation of structure and dynamics during phase separation of an elastomeric protein, *Proc. Natl. Acad. Sci.* 201701877 (2017).
- [15] L. Eisoltd, J.G. Hardy, M. Heim, T. Scheibel, The role of salt and shear on the storage and assembly of spider silk proteins, *J. Struct. Biol.* 170 (2010) 413–419, <https://doi.org/10.1016/j.jsb.2009.12.027>.
- [16] F. Hagn, L. Eisoltd, J.G. Hardy, C. Vendrely, M. Coles, T. Scheibel, H. Kessler, A conserved spider silk domain acts as a molecular switch that controls fibre assembly, *Nature* 465 (2010) 239–242, <https://doi.org/10.1038/nature08936>.
- [17] R. Mezzenga, P. Fischer, The self-assembly, aggregation and phase transitions of food protein systems in one, two and three dimensions, *Rep. Prog. Phys.* 76 (2013), <https://doi.org/10.1088/0034-4885/76/4/046601>.
- [18] W. Wei, L. Petrone, Y. Tan, H. Cai, J.N. Israelachvili, A. Miserez, J.H. Waite, An underwater surface-drying peptide inspired by a mussel adhesive protein, *Adv. Funct. Mater.* 26 (2016) 3496–3507, <https://doi.org/10.1002/adfm.201600210>.
- [19] A.B. Kayitmazer, Thermodynamics of complex coacervation, *Adv. Colloid Interface Sci.* 239 (2017) 169–177, <https://doi.org/10.1016/j.jcis.2016.07.006>.

- [20] S. Rammensee, U. Slotta, T. Scheibel, A.R. Bausch, Assembly mechanism of recombinant spider silk proteins, *Proc. Natl. Acad. Sci. USA* 105 (2008) 6590–6595, <https://doi.org/10.1073/pnas.0709246105>.
- [21] Y. Zhang, P.S. Cremer, Interactions between macromolecules and ions: the Hofmeister series, *Curr. Opin. Chem. Biol.* 10 (2006) 658–663.
- [22] W. Kunz, Specific ion effects in colloidal and biological systems, *Curr. Opin. Colloid Interface Sci.* 15 (2010) 34–39.
- [23] P. Lo Nostro, B.W. Ninham, Hofmeister phenomena: an update on ion specificity in biology, *Chem. Rev.* 112 (2012) 2286–2322.
- [24] D.P. Knight, F. Vollrath, Changes in element composition along the spinning duct in a *Nephila* spider, *Naturwissenschaften* 88 (2001) 179–182.
- [25] S. Lim, D. Moon, H.J. Kim, J.H. Seo, I.S. Kang, H.J. Cha, Interfacial tension of complex coacervated mussel adhesive protein according to the Hofmeister series, *Langmuir* 30 (2014) 1108–1115.
- [26] S. Kim, H.Y. Yoo, J. Huang, Y. Lee, S. Park, Y. Park, S. Jin, Y.M. Jung, H. Zeng, D.S. Hwang, Y. Jho, Salt triggers the simple coacervation of an underwater adhesive when cations meet aromatic? Electrons in seawater, *ACS Nano* (2017), <https://doi.org/10.1021/acsnano.7b01370>.
- [27] P. Mohammadi, A.S. Aranko, L. Lemetti, Z. Cenev, Q. Zhou, S. Virtanen, C.P. Landowski, M. Penttilä, W.J. Fischer, W. Wagermaier, M.B. Linder, Phase transitions as intermediate steps in the formation of molecularly engineered protein fibers, *Commun. Biol.* 1 (2018) 86, <https://doi.org/10.1038/s42003-018-0090-y>.
- [28] W. Fang, M. Nonappa, P. Vitikainen, S. Mohammadi, M. Koskela, A. Soikkeli, C.P. Westerholm-Parvinen, M. Landowski, M.B. Penttilä, P. Laaksonen Linder, Coacervation of resilin fusion proteins containing terminal functionalities, *Colloids Surf. B Biointerfaces* (2018), <https://doi.org/10.1016/j.colsurfb.2018.07.048>.
- [29] P. Mohammadi, G. Beaune, B.T. Stokke, J.V.I. Timonen, M.B. Linder, Self-coacervation of a silk-like protein and its use as an adhesive for cellulosic materials, *ACS Macro Lett.* (2018) 1120–1125, <https://doi.org/10.1021/acsmacrolett.8b00527>.
- [30] P. Mohammadi, A.S. Aranko, C.P. Landowski, O. Ikkala, K. Jaudzems, W. Wagermaier, M. Linder, Biomimetic composites with enhanced toughening using silk-inspired triblock proteins and aligned nanocellulose reinforcements, *Sci. Adv.* (2019) 5.
- [31] R.P. Sear, Nucleation: theory and applications to protein solutions and colloidal suspensions, *J. Phys. Condens. Matter.* 19 (2007) 33101.
- [32] V.V. Slezov, Kinetics of first order phase transitions, John Wiley & Sons, 2009.
- [33] V.I. Kalikmanov, Classical nucleation theory, in: *Nucleation Theory*, Springer, 2013, pp. 17–41.
- [34] S. Karthika, T.K. Radhakrishnan, P. Kalaichelvi, A review of classical and nonclassical nucleation theories, *Cryst. Growth Des.* 16 (2016) 6663–6681.
- [35] H. Le Ferrand, M. Duchamp, B. Gabryelczyk, H. Cai, A. Miserez, Time-resolved observations of liquid-liquid phase separation at the nanoscale using in situ liquid transmission electron microscopy, *J. Am. Chem. Soc.* (2019).
- [36] H. Vehkamäki, *Classical nucleation theory in multicomponent systems*, Springer Science & Business Media, 2006.
- [37] S. Kim, J. Huang, Y. Lee, S. Dutta, H.Y. Yoo, Y.M. Jung, Y. Jho, H. Zeng, D.S. Hwang, Complexation and coacervation of like-charged polyelectrolytes inspired by mussels, *Proc. Natl. Acad. Sci.* 113 (2016) E847–E853.
- [38] D.S. Hwang, H. Zeng, A. Srivastava, D.V. Krogstad, M. Tirrell, J.N. Israelachvili, J. H. Waite, Viscosity and interfacial properties in a mussel-inspired adhesive coacervate, *Soft Matter* 6 (2010) 3232–3236.
- [39] F.M. Menger, A.V. Peresyppkin, K.L. Caran, R.P. Apkarian, A sponge morphology in an elementary coacervate, *Langmuir* (2000) 9113–9116, <https://doi.org/10.1021/la0010626>.
- [40] H. LeVine III, [18] Quantification of β -sheet amyloid fibril structures with thioflavin T, in: *Methods Enzymol*, Elsevier, 1999, pp. 274–284.
- [41] J. Lee, E.K. Culyba, E.T. Powers, J.W. Kelly, Amyloid- β forms fibrils by nucleated conformational conversion of oligomers, *Nat. Chem. Biol.* 7 (2011) 602.
- [42] A. Lakshmanan, D.W. Cheong, A. Accardo, E. Di Fabrizio, C. Riekel, C.A.E. Hauser, Aliphatic peptides show similar self-assembly to amyloid core sequences, challenging the importance of aromatic interactions in amyloidosis, *Proc. Natl. Acad. Sci.* 110 (2013) 519–524.
- [43] D. Huemmerich, C.W. Helsen, S. Quedzuweit, J. Oschmann, J. Rudolph, T. Scheibel, Primary structure elements of spider dragline silks and their contribution to protein solubility, *Biochemistry* 43 (2004) 13604–13612.
- [44] P.A. Guerette, D.G. Ginzinger, B.H. Weber, J.M. Gosline, Silk properties determined by gland-specific expression of a spider fibroin gene family, *Science* 272 (1996) 112–115, <https://doi.org/10.1126/science.272.5258.112>.
- [45] J.M. Gosline, P.A. Guerette, C.S. Ortlepp, K.N. Savage, The mechanical design of spider silks: from fibroin sequence to mechanical function, *J. Exp. Biol.* 202 (1999) 3295–3303.
- [46] P.E. Wright, H.J. Dyson, Intrinsically disordered proteins in cellular signalling and regulation, *Nat. Rev. Mol. Cell Biol.* 16 (2015) 18.
- [47] A.J. Baldwin, L.E. Kay, NMR spectroscopy brings invisible protein states into focus, *Nat. Chem. Biol.* 5 (2009) 808.
- [48] J.P. Brady, P.J. Farber, A. Sekhar, Y.-H. Lin, R. Huang, A. Bah, T.J. Nott, H.S. Chan, A.J. Baldwin, J.D. Forman-Kay, Structural and hydrodynamic properties of an intrinsically disordered region of a germ cell-specific protein on phase separation, *Proc. Natl. Acad. Sci.* 114 (2017) E8194–E8203.
- [49] D.T. Murray, M. Kato, Y. Lin, K.R. Thurber, I. Hung, S.L. McKnight, R. Tycko, Structure of FUS protein fibrils and its relevance to self-assembly and phase separation of low-complexity domains, *Cell* 171 (2017) 615–627.
- [50] S. Xiang, M. Kato, L.C. Wu, Y. Lin, M. Ding, Y. Zhang, Y. Yu, S.L. McKnight, The LC domain of hnRNPA2 adopts similar conformations in hydrogel polymers, liquid-like droplets, and nuclei, *Cell* 163 (2015) 829–839.
- [51] S.B. Kennedy, E.R. DeAzevedo, W.A. Petka, T.P. Russell, D.A. Tirrell, M. Hong, Dynamic structure of a protein hydrogel: a solid-state NMR study, *Macromolecules* 34 (2001) 8675–8685.
- [52] C. Ader, S. Frey, W. Maas, H.B. Schmidt, D. Görlich, M. Baldus, Amyloid-like interactions within nucleoporin FG hydrogels, *Proc. Natl. Acad. Sci.* 107 (2010) 6281–6285.
- [53] J.D. Van Beek, L. Beaulieu, H. Schäfer, M. Demura, T. Asakura, B.H. Meier, Solid-state NMR determination of the secondary structure of *Samia cynthia ricini* silk, *Nature* 405 (2000) 1077.
- [54] B.A. Lawrence, C.A. Vierra, A.M.F. Moore, Molecular and mechanical properties of major ampullate silk of the black widow spider, *Latrodectus hesperus*, *Biomacromolecules* 5 (2004) 689–695.
- [55] D.H. Hijirida, K.G. Do, C. Michal, L.W. Jelinski, ¹³C NMR of *nephila clavipes* major ampullate silk, *Gland* 71 (1996) 3442–3447, [https://doi.org/10.1016/S0006-3495\(96\)79539-5](https://doi.org/10.1016/S0006-3495(96)79539-5).
- [56] Yongdae Shin, Clifford P. Brangwynne, Liquid phase condensation in cell physiology and disease, *Science* 357 (6357) (2017) eaaf4382, <https://doi.org/10.1126/science.aaf4382>.
- [57] E. Stroo, M. Koopman, E.A.A. Nollen, A. Mata-Cabana, Cellular regulation of amyloid formation in aging and disease, *Front. Neurosci.* 11 (2017) 64.
- [58] J.R. Simon, N.J. Carroll, M. Rubinstein, A. Chilkoti, G.P. López, Programming molecular self-assembly of intrinsically disordered proteins containing sequences of low complexity, *Nat. Chem.* 9 (2017) 509.
- [59] J. Tormo, R. Lamed, A.J. Chirino, E. Morag, E.A. Bayer, Y. Shoham, T.A. Steitz, Crystal structure of a bacterial family-III cellulose-binding domain: a general mechanism for attachment to cellulose, *EMBO J.* 15 (1996) 5739.
- [60] M. Hedhammar, A. Rising, S. Grip, A.S. Martinez, K. Nordling, C. Casals, M. Stark, J. Johansson, Structural properties of recombinant nonrepetitive and repetitive parts of major ampullate spidroin 1 from *Euprostheno australis*: implications for fiber formation, *Biochemistry* 47 (2008) 3407–3417.
- [61] C. Engler, R. Kandzia, S. Marillonnet, A one pot, one step, precision cloning method with high throughput capability, *PLoS ONE* 3 (2008) e3647.
- [62] N.E. Sanjana, L. Cong, Y. Zhou, M.M. Cunniff, G. Feng, F. Zhang, A transcription activator-like effector toolbox for genome engineering, *Nat. Protoc.* 7 (2012) 171–192.
- [63] P. Yan, X. Gao, W. Shen, P. Zhou, J. Duan, Parallel assembly for multiple site-directed mutagenesis of plasmids, *Anal. Biochem.* 430 (2012) 65–67.
- [64] C.A. Schneider, W.S. Rasband, K.W. Eliceiri, NIH Image to ImageJ: 25 years of image analysis, *Nat. Methods.* 9 (2012) 671–675.
- [65] J. Schindelin, I. Arganda-Carreras, E. Frise, V. Kaynig, M. Longair, T. Pietzsch, S. Preibisch, C. Rueden, S. Saalfeld, B. Schmid, Fiji: an open-source platform for biological-image analysis, *Nat. Methods.* 9 (2012) 676–682.
- [66] E. Gasteiger, C. Hoogland, A. Gattiker, S. Duvaud, M.R. Wilkins, R.D. Appel, A. Bairoch, John M. Walker (ed.), *The proteomics protocols handbook* (2005).